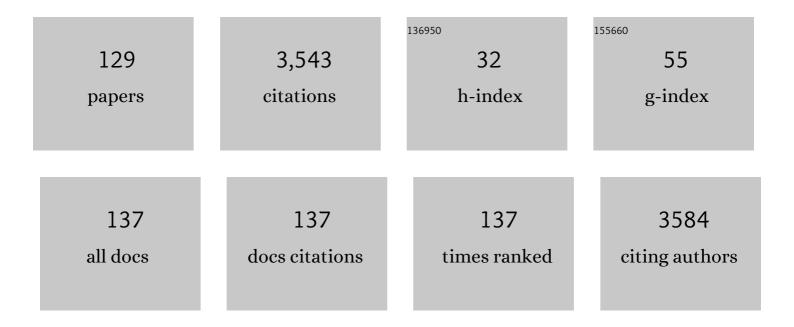
Andrea Somogyi

List of Publications by Year in descending order

Source: https://exaly.com/author-pdf/4222236/publications.pdf Version: 2024-02-01



#	Article	IF	CITATIONS
1	From visible light to X-ray microscopy: major steps in the evolution of developmental models for calcification of invertebrate skeletons. Comptes Rendus Chimie, 2022, 25, 577-595.	0.5	0
2	Synchrotron-Based HR-Fluorescence and Mineralogical Mapping of the Initial Growth Stages of Polynesian Cultivated Pearls Disprove the â€~Reversed Shell' Concept. Minerals (Basel, Switzerland), 2022, 12, 172.	2.0	2
3	Intracellular bound chlorophyll residues identify 1 Gyr-old fossils as eukaryotic algae. Nature Communications, 2022, 13, 146.	12.8	18
4	Cellular Detection of a Mitochondria Targeted Brominated Vinyl Triphenylamine Optical Probe (TPâ^'Br) by Xâ€Ray Fluorescence Microscopy. Chemistry - A European Journal, 2022, 28, .	3.3	3
5	Pathologies related to abnormal deposits in dermatology: a physico-chemical approach. Comptes Rendus Chimie, 2022, 25, 445-476.	0.5	10
6	Cytoplasmic aggregation of uranium in human dopaminergic cells after continuous exposure to soluble uranyl at non-cytotoxic concentrations. NeuroToxicology, 2021, 82, 35-44.	3.0	3
7	Rhenium carbonyl complexes bearing methylated triphenylphosphonium cations as antibody-free mitochondria trackers for X-ray fluorescence imaging. Inorganic Chemistry Frontiers, 2021, 8, 3905-3915.	6.0	13
8	Uranium incorporation in fluorite and exploration of U–Pb dating. Geochronology, 2021, 3, 199-227.	2.5	10
9	Correlative optical photothermal infrared and X-ray fluorescence for chemical imaging of trace elements and relevant molecular structures directly in neurons. Light: Science and Applications, 2021, 10, 151.	16.6	24
10	Catabolism of lysosome-related organelles in color-changing spiders supports intracellular turnover of pigments. Proceedings of the National Academy of Sciences of the United States of America, 2021, 118, .	7.1	10
11	SOLEIL'S Process Automation Improvement Using Industrial Robots. Synchrotron Radiation News, 2021, 34, 10-17.	0.8	0
12	Foraminiferal Mn/Ca as Bottomâ€Water Hypoxia Proxy: An Assessment of <i>Nonionella stella</i> in the Santa Barbara Basin, USA. Paleoceanography and Paleoclimatology, 2021, 36, e2020PA004167.	2.9	5
13	Nonâ€spherical pearl layers in the Polynesian â€`blackâ€lipped' <i>Pinctada margaritifera</i> : The nonâ€nacreous deposits compared to microstructure of the shell growing edge. Aquaculture Research, 2020, 51, 506-522.	1.8	4
14	Early diagenesis of foraminiferal calcite under anoxic conditions: A case study from the Landsort Deep, Baltic Sea (IODP Site M0063). Chemical Geology, 2020, 558, 119871.	3.3	4
15	Broadband coherent diffractive imaging. Nature Photonics, 2020, 14, 618-622.	31.4	29
16	Resolving Internal Structures and Composition of Biominerals: The Case of Calcitic Prisms of Mollusk Shells. Microscopy and Microanalysis, 2020, 26, 96-98.	0.4	1
17	Modern arsenotrophic microbial mats provide an analogue for life in the anoxic Archean. Communications Earth & Environment, 2020, 1, .	6.8	24
18	Intracellular location matters: rationalization of the anti-inflammatory activity of a manganese(<scp>ii</scp>) superoxide dismutase mimic complex. Chemical Communications, 2020, 56, 7885-7888.	4.1	16

#	Article	IF	CITATIONS
19	Geochemical evidence for arsenic cycling in living microbialites of a High Altitude Andean Lake (Laguna Diamante, Argentina). Chemical Geology, 2020, 549, 119681.	3.3	11
20	Anti-inflammatory activity of superoxide dismutase mimics functionalized with cell-penetrating peptides. Dalton Transactions, 2020, 49, 2323-2330.	3.3	17
21	Trace element perspective into the ca. 2.1-billion-year-old shallow-marine microbial mats from the Francevillian Group, Gabon. Chemical Geology, 2020, 543, 119620.	3.3	3
22	Inside black pearls. Materials Characterization, 2020, 163, 110276.	4.4	3
23	Manganese Mapping Using a Fluorescent Mn ²⁺ Sensor and Nanosynchrotron X-ray Fluorescence Reveals the Role of the Golgi Apparatus as a Manganese Storage Site. Inorganic Chemistry, 2019, 58, 13724-13732.	4.0	23
24	Microbially induced potassium enrichment in Paleoproterozoic shales and implications for reverse weathering on early Earth. Nature Communications, 2019, 10, 2670.	12.8	17
25	The rise of oxygen-driven arsenic cycling at ca. 2.48 Ga. Geology, 2019, 47, 243-246.	4.4	27
26	Detection of titanium nanoparticles in the hair shafts of a patient with frontal fibrosing alopecia. Journal of the European Academy of Dermatology and Venereology, 2018, 32, e442-e443.	2.4	21
27	Graftable SCoMPIs enable the labeling and X-ray fluorescence imaging of proteins. Chemical Science, 2018, 9, 4483-4487.	7.4	15
28	Fast full-field micro-tomography at the Nanoscopium multitechnique nanoprobe beamline of Synchrotron Soleil. Microscopy and Microanalysis, 2018, 24, 254-255.	0.4	6
29	The Prismatic Layer of Pinna: A Showcase of Methodological Problems and Preconceived Hypotheses. Minerals (Basel, Switzerland), 2018, 8, 365.	2.0	8
30	Revisiting the Organic Template Model through the Microstructural Study of Shell Development in Pinctada margaritifera, the Polynesian Pearl Oyster. Minerals (Basel, Switzerland), 2018, 8, 370.	2.0	13
31	Estimated Performance of Nanoscopium at an Upgraded Synchrotron Soleil Microscopy and Microanalysis, 2018, 24, 258-259.	0.4	1
32	Distribution, redox state and (bio)geochemical implications of arsenic in present day microbialites of Laguna Brava, Salar de Atacama. Chemical Geology, 2018, 490, 13-21.	3.3	41
33	Patterns of metal distribution in hypersaline microbialites during early diagenesis: Implications for the fossil record. Geobiology, 2017, 15, 259-279.	2.4	40
34	MMX-I: A data-processing software for multi-modal X-ray imaging and tomography. Journal of Physics: Conference Series, 2017, 849, 012060.	0.4	1
35	Development and operation of a <mmi:math xmins:mmi="http://www.w3.org/1998/Math/Math/Math/M<br">display="inline"><mml:mrow><mml:mrow><mml:msub><mml:mrow><mml:mi>Pr</mml:mi></mml:mrow><mm mathvariant="normal">B</mm </mml:msub></mml:mrow> based cryogenic permanent magnet undulator for a high spatial resolution x-ray beam line. Physical Review Accelerators and Beams, 2017,</mml:mrow></mmi:math>	l:mrow> <r 1.6</r 	mml:mn>2< 36
36	20, Arsenic distribution and valence state variation studied by fast hierarchical length-scale morphological, compositional, and speciation imaging at the Nanoscopium, Synchrotron Soleil. , 2017, , .		0

#	Article	IF	CITATIONS
37	Rapid and reliable diagnosis of Wilson disease using Xâ€ray fluorescence. Journal of Pathology: Clinical Research, 2016, 2, 175-186.	3.0	18
38	Fabrication and characterization of high-efficiency double-sided blazed x-ray optics. Optics Letters, 2016, 41, 281.	3.3	20
39	<i>MMX-I</i> : data-processing software for multimodal X-ray imaging and tomography. Journal of Synchrotron Radiation, 2016, 23, 783-794.	2.4	13
40	Optical design and multi-length-scale scanning spectro-microscopy possibilities at the NanoscopiumÂbeamline of Synchrotron Soleil. Journal of Synchrotron Radiation, 2015, 22, 1118-1129.	2.4	67
41	High resolution double-sided diffractive optics for hard X-ray microscopy. Optics Express, 2015, 23, 776.	3.4	46
42	Possibilities and Challenges of Scanning Hard X-ray Spectro-microscopy Techniques in Material Sciences. AIMS Materials Science, 2015, 2, 122-162.	1.4	7
43	High-efficiency zone-plate optics for multi-keV X-ray focusing. Journal of Synchrotron Radiation, 2014, 21, 497-501.	2.4	48
44	Evidence for arsenic metabolism and cycling by microorganisms 2.7 billion years ago. Nature Geoscience, 2014, 7, 811-815.	12.9	100
45	High efficiency x-ray nanofocusing by the blazed stacking of binary zone plates. Proceedings of SPIE, 2013, , .	0.8	6
46	Design optimization of ultra-precise elliptical mirrors for hard x-ray nanofocusing at Nanoscopium. Proceedings of SPIE, 2013, , .	0.8	1
47	Status of the Nanoscopium scanning nanoprobe beamline of Synchrotron Soleil. Proceedings of SPIE, 2013, , .	0.8	1
48	Simultaneous fast scanning XRF, dark field, phase-, and absorption contrast tomography. Proceedings of SPIE, 2013, , .	0.8	0
49	Development of fast, simultaneous and multi-technique scanning hard X-ray microscopy at Synchrotron Soleil. Journal of Synchrotron Radiation, 2013, 20, 293-299.	2.4	47
50	Status of the Nanoscopium Scanning Hard X-ray Nanoprobe Beamline of Synchrotron Soleil. Journal of Physics: Conference Series, 2013, 463, 012027.	0.4	3
51	Development of fast parallel multi-technique scanning X-ray imaging at Synchrotron Soleil. Journal of Physics: Conference Series, 2013, 463, 012031.	0.4	7
52	Parabolic crossed planar polymeric x-ray lenses. Journal of Micromechanics and Microengineering, 2011, 21, 015020.	2.6	23
53	The Scanning Nanoprobe Beamline Nanoscopium at Synchrotron Soleil. AIP Conference Proceedings, 2011, , .	0.4	9
54	Nanoscopium: a Scanning Hard X-ray Nanoprobe Beamline at Synchrotron Soleil. AIP Conference Proceedings, 2010, , .	0.4	8

#	Article	IF	CITATIONS
55	Inversion domain boundaries in GaN studied by Xâ€ray microprobe. Physica Status Solidi - Rapid Research Letters, 2010, 4, 31-33.	2.4	0
56	Bromine cycle in subduction zones through in situ Br monitoring in diamond anvil cells. Geochimica Et Cosmochimica Acta, 2010, 74, 3839-3850.	3.9	41
57	Very first tests on SOLEIL regarding the Zn environment in pathological calcifications made of apatite determined by X-ray absorption spectroscopy. Journal of Synchrotron Radiation, 2008, 15, 506-509.	2.4	37
58	Microanalysis (Micro-XRF, Micro-XANES, and Micro-XRD) of a Tertiary Sediment Using Microfocused Synchrotron Radiation. Microscopy and Microanalysis, 2007, 13, 165-172.	0.4	34
59	<i>In situ</i> mapping of high-pressure fluids using hydrothermal diamond anvil cells. High Pressure Research, 2007, 27, 235-247.	1.2	17
60	Formation of Si clusters in AlGaN: A study of local structure. Applied Physics Letters, 2007, 90, 181129.	3.3	9
61	Trace element distribution in annual stalagmite laminae mapped by micrometer-resolution X-ray fluorescence: Implications for incorporation of environmentally significant species. Geochimica Et Cosmochimica Acta, 2007, 71, 1494-1512.	3.9	205
62	Determination of the Cd-Bearing Phases in Municipal Solid Waste and Biomass Single Fly Ash Particles Using SR-μXRF Spectroscopy. Analytical Chemistry, 2007, 79, 6496-6506.	6.5	16
63	Confocal μ-XRF, μ-XAFS, and μ-XRD Studies of Sediment from a Nuclear Waste Disposal Natural Analogue Site and Fractured Granite Following a Radiotracer Migration Experiment. AIP Conference Proceedings, 2007, , .	0.4	4
64	3D imaging of vapour and liquid inclusions from the Mole Granite, Australia, using helical fluorescence tomography. Spectrochimica Acta, Part B: Atomic Spectroscopy, 2007, 62, 799-806.	2.9	10
65	X-ray transmission properties of intelligent anvils in diamond anvil cells. High Pressure Research, 2006, 26, 235-241.	1.2	4
66	Standardless quantification of single fluid inclusions using synchrotron radiation induced X-ray fluorescence. Chemical Geology, 2006, 227, 165-183.	3.3	20
67	Synchrotron X-rays in situ analysis of extraterrestrial grains trapped in aerogel. Advances in Space Research, 2006, 38, 2068-2074.	2.6	5
68	Crystal fragmentation and columnar-to-equiaxed transitions in Al-Cu studied by synchrotron X-ray video microscopy. Metallurgical and Materials Transactions A: Physical Metallurgy and Materials Science, 2006, 37, 2515-2524.	2.2	170
69	Multielement Si(Li) detector for the hard x-ray microprobe at ID22 (ESRF). Review of Scientific Instruments, 2006, 77, 063705.	1.3	10
70	Scanning x-ray excited optical luminescence microscopy in GaN. Applied Physics Letters, 2006, 89, 221913.	3.3	50
71	Methodological Study Using XAS of an ArsenicBased Antileukemia Treatment. Physica Scripta, 2005, , 870.	2.5	3
72	CLIMATE FORCINGS AND THEIR INFLUENCE ON ALPINE HISTORY AS RECONSTRUCTED THROUGH THE APPLICATION OF SYNCHROTRON-BASED X-RAY MICROFLUORESCENCE ON LAYERED STALAGMITES*. Archaeometry, 2005, 47, 209-219.	1.3	10

#	Article	IF	CITATIONS
73	ID22: a multitechnique hard X-ray microprobe beamline at the European Synchrotron Radiation Facility. Journal of Synchrotron Radiation, 2005, 12, 208-215.	2.4	44
74	In Situ Speciation of Nickel in Hydrous Melts Exposed toExtreme Conditions. Physica Scripta, 2005, , 921.	2.5	3
75	Micro-x-ray absorption near-edge structure imaging for detecting metallic Mn in GaN. Applied Physics Letters, 2005, 87, 061913.	3.3	25
76	Mn-rich clusters in GaN: Hexagonal or cubic symmetry?. Applied Physics Letters, 2005, 86, 131927.	3.3	58
77	Detection of a Ca-rich lithology in the Earth's deep (>300 km) convecting mantle. Earth and Planetary Science Letters, 2005, 236, 579-587.	4.4	90
78	Beryllium parabolic refractive x-ray lenses. AIP Conference Proceedings, 2004, , .	0.4	18
79	Nondestructive three-dimensional elemental microanalysis by combined helical x-ray microtomographies. Applied Physics Letters, 2004, 84, 2199-2201.	3.3	54
80	Direct Observation of Mn Clusters in GaN by X-ray Scanning Microscopy. Japanese Journal of Applied Physics, 2004, 43, L695-L697.	1.5	11
81	Nanofocusing Parabolic Refractive X-Ray Lenses. AIP Conference Proceedings, 2004, , .	0.4	7
82	Characterization of impact materials around Barringer Meteor Crater by micro-PIXE and micro-SRXRF techniques. Nuclear Instruments & Methods in Physics Research B, 2004, 219-220, 555-560.	1.4	8
83	Three-Dimensional Trace Element Analysis by Confocal X-ray Microfluorescence Imaging. Analytical Chemistry, 2004, 76, 6786-6791.	6.5	237
84	Effects of Strontium on the Physicochemical Characteristics of Hydroxyapatite. Calcified Tissue International, 2004, 75, 405-415.	3.1	89
85	Focusing X-rays with simple arrays of prism-like structures. Journal of Synchrotron Radiation, 2004, 11, 248-253.	2.4	39
86	A library for X-ray–matter interaction cross sections for X-ray fluorescence applications. Spectrochimica Acta, Part B: Atomic Spectroscopy, 2004, 59, 1725-1731.	2.9	128
87	Voxel-based Monte Carlo simulation of X-ray imaging and spectroscopy experiments. Spectrochimica Acta, Part B: Atomic Spectroscopy, 2004, 59, 1747-1754.	2.9	53
88	Application of combined micro-proton-induced X-ray emission and micro-synchrotron radiation X-ray fluorescence techniques for the characterization of impact materials around Barringer Meteor Crater. Spectrochimica Acta, Part B: Atomic Spectroscopy, 2004, 59, 1717-1723.	2.9	4
89	Microanalysis study of archaeological mural samples containing Maya blue pigment. Spectrochimica Acta, Part B: Atomic Spectroscopy, 2004, 59, 1619-1625.	2.9	60
90	Micro-XANES and X-ray microtomography study of oxidation State, morphology, and chemistry evolution during nuclear fuel sintering. IEEE Transactions on Nuclear Science, 2004, 51, 1657-1661.	2.0	8

#	Article	IF	CITATIONS
91	Quantification of Single Fluid Inclusions by Combining Synchrotron Radiation-Induced μ-X-ray Fluorescence and Transmission. Analytical Chemistry, 2004, 76, 3988-3994.	6.5	19
92	Microchemical Element Imaging of Yeast and Human Cells Using Synchrotron X-ray Microprobe with Kirkpatrickâ^'Baez Optics. Analytical Chemistry, 2004, 76, 309-314.	6.5	46
93	X-ray Fluorescence Tomography of Individual Municipal Solid Waste and Biomass Fly Ash Particles. Analytical Chemistry, 2004, 76, 1586-1595.	6.5	31
94	Microextended X-ray Absorption Fine Structure Studies of Cadmium Speciation within Single Municipal Solid Waste Fly Ash Particles. Analytical Chemistry, 2004, 76, 1596-1602.	6.5	15
95	High-resolution imaging of sulfur oxidation states, trace elements, and organic molecules distribution in individual microfossils and contempo rary microbial filaments 1 1Associate editor: N. E. Ostrom. Geochimica Et Cosmochimica Acta, 2004, 68, 1561-1569.	3.9	30
96	Biological control of Cl/Br and low sulfate concentration in a 3.5-Gyr-old seawater from North Pole, Western Australia. Earth and Planetary Science Letters, 2004, 228, 451-463.	4.4	82
97	Seven years of x-ray fluorescence computed microtomography. , 2004, , .		6
98	Nanotomography using parabolic refractive x-ray lenses. , 2004, 5535, 701.		5
99	Focusing hard x-rays with large kinoform lenses of mm size. , 2004, , .		0
100	Planar sets of cross x-ray refractive lenses from SU-8 polymer. , 2004, , .		30
101	Fluorescence microtomography using nanofocusing refractive x-ray lenses. , 2004, , .		4
102	Tomography with chemical speciation. , 2004, 5535, 29.		0
103	Quantitative X-ray fluorescence analysis at the ESRF ID18F microprobe. Nuclear Instruments & Methods in Physics Research B, 2003, 199, 396-401.	1.4	16
104	Effects of beamline components (undulator, monochromator, focusing device) on the beam intensity at ID18F (ESRF). Nuclear Instruments & Methods in Physics Research B, 2003, 199, 559-564.	1.4	11
105	Microimaging and tomography with chemical speciation. Nuclear Instruments & Methods in Physics Research B, 2003, 200, 444-450.	1.4	47
106	Miniature ionization chamber detector developed for X-ray microprobe measurements. Journal of Synchrotron Radiation, 2003, 10, 187-190.	2.4	11
107	Micro-heterogeneity study of trace elements in USGS, MPI-DING and NIST glass reference materials by means of synchrotron micro-XRF. Journal of Analytical Atomic Spectrometry, 2003, 18, 350-357.	3.0	46
108	Internal elemental microanalysis combining x-ray fluorescence, Compton and transmission tomography. Journal of Applied Physics, 2003, 94, 145-156.	2.5	142

#	Article	IF	CITATIONS
109	Nanofocusing parabolic refractive x-ray lenses. Applied Physics Letters, 2003, 82, 1485-1487.	3.3	178
110	The Xâ€ray Microscopy and Microâ€spectroscopy facility at the ESRF. Synchrotron Radiation News, 2003, 16, 35-43.	0.8	6
111	X-ray fluorescence tomography of individual waste fly ash particles. European Physical Journal Special Topics, 2003, 104, 647-650.	0.2	6
112	Focusing of hard X-rays using diamond and silicon refractive lenses. European Physical Journal Special Topics, 2003, 104, 223-226.	0.2	1
113	In situ SXRF determination of Pb partitioning in hydrothermal Diamond Anvil Cell. European Physical Journal Special Topics, 2003, 104, 391-391.	0.2	1
114	Direct Determination of Cadmium Speciation in Municipal Solid Waste Fly Ashes by Synchrotron Radiation Induced μ-X-ray Fluorescence and μ-X-ray Absorption Spectroscopy. Environmental Science & Technology, 2002, 36, 3165-3169.	10.0	42
115	Quantitative Trace Element Analysis of Individual Fly Ash Particles by Means of X-ray Microfluorescence. Analytical Chemistry, 2002, 74, 1128-1135.	6.5	56
116	A Monte Carlo Model for Studying the Microheterogeneity of Trace Elements in Reference Materials by Means of Synchrotron Microscopic X-ray Fluorescence. Analytical Chemistry, 2002, 74, 5017-5026.	6.5	26
117	XANES micro-imaging and tomography. , 2002, , .		13
118	Synchrotron radiation induced μ-X-ray fluorescence spectroscopy on municipal solid waste fly ashes. Spectrochimica Acta, Part B: Atomic Spectroscopy, 2001, 56, 1355-1365.	2.9	18
119	ID18F: a new micro-x-ray fluorescence end-station at the European Synchrotron Radiation Facility (ESRF): preliminary results. X-Ray Spectrometry, 2001, 30, 242-252.	1.4	84
120	In situ radiotracer and voltammetric study of Zn electrosorption on noble metal electrodes. Journal of Electroanalytical Chemistry, 2000, 485, 121-127.	3.8	6
121	Interpretation and use of inter-element correlation graphs obtained by scanning X-ray fluorescence micro-beam spectrometry from individual particles. Part II — application. Spectrochimica Acta, Part B: Atomic Spectroscopy, 2000, 55, 1039-1049.	2.9	7
122	Interpretation and use of inter-element correlation graphs obtained by scanning X-ray fluorescence micro-beam spectrometry from individual particles. Part I — theory. Spectrochimica Acta, Part B: Atomic Spectroscopy, 2000, 55, 75-89.	2.9	12
123	Investigation of geochemical composition of lake sediments using ED-XRF and ICP-AES techniques. X-Ray Spectrometry, 1999, 28, 399-405.	1.4	32
124	Investigation of lead transport effect from glazed pottery to liquid medium by EDXRF and ICP-AES methods. Journal of Analytical Atomic Spectrometry, 1999, 14, 479-482.	3.0	8
125	Speciation of elements in lake sediments investigated using x-ray fluorescence and inductively coupled plasma atomic emission spectrometry. X-Ray Spectrometry, 1998, 27, 283-287.	1.4	10
126	Comparison between X-ray fluorescence and inductively coupled plasma atomic emission spectrometry in the analysis of sediment samples. Spectrochimica Acta, Part B: Atomic Spectroscopy, 1997, 52, 2011-2017.	2.9	14

#	Article	IF	CITATIONS
127	Comparison of emission-transmission and elemental sensitivity Methods for determining the trace element content of biological samples. X-Ray Spectrometry, 1995, 24, 193-200.	1.4	4
128	Determination of incident angle in radioisotope-excited EDXRF. X-Ray Spectrometry, 1993, 22, 395-400.	1.4	5
129	Air concentrations of Chernobyl fallout radionuclides in the area Debrecen (Hungary). Acta Physica Hungarica, 1991, 69, 309-319.	0.1	6